


ARTICLE

DOI: 10.1038/s42005-018-0045-0

OPEN

Femtosecond pulse generation beyond photon lifetime limit in gain-switched semiconductor lasers

Takashi Ito ¹, Hidekazu Nakamae¹, Yuji Hazama¹, Takahiro Nakamura¹, Shaoqiang Chen², Masahiro Yoshita³, Changsu Kim¹, Yohei Kobayashi¹ & Hidefumi Akiyama¹

Femtosecond semiconductor lasers are ideal devices to provide the ultrashort pulses for industrial and biomedical use because of their robustness, stability, compactness and potential low cost. In particular, gain-switched semiconductor lasers have significant advantages of flexible pulse shaping and repetition rate with the robustness. Here we first demonstrate our laser, which is initiated by very strong pumping of 100 times the lasing threshold density, can surpass the photon lifetime limit that has restricted the pulse width to picoseconds for the past four decades and produce an unprecedented ultrashort pulse of 670 fs with a peak power of 7.5 W on autocorrelation measurement. The measured phenomena are reproduced effectively by our numerical calculation based on rate equations including the non-equilibrium intraband carrier distribution, which reveal that the pulse width is limited by the carrier-carrier scattering time, instead of the photon lifetime.

¹Institute for Solid State Physics, University of Tokyo, Chiba, Kashiwa 277-8581, Japan. ²Department of Electronic Engineering, East China Normal University, 200241 Shanghai, China. ³National Institute of Advanced Industrial Science and Technology, Ibaraki, Tsukuba 305-8568, Japan. Correspondence and requests for materials should be addressed to T.I. (email: ito@issp.u-tokyo.ac.jp)

Femtosecond lasers and amplifiers provide high field energy densities by concentrating optical fields in both the temporal and spatial domains, which induces novel light-matter non-linear interactions, enabling innovative applications such as non-thermal laser processing, super-resolution multi-photon three-dimensional microscopy and biomedical microsurgery. Currently, mode-locked (ML) fibre lasers are the most useful for these applications due to their high stability and durability. However, under severe environmental conditions with temperature fluctuations, vibrations and other disturbances, crucial instabilities occur in their ML operation, because non-linear effects in the laser cavities such as non-linear-polarization rotation are sensitive to these perturbations. Degradation of saturable absorbers is another serious problem.

Femtosecond semiconductor lasers should be the ideal choice for industrial and biomedical use because of their robustness, stability, compactness and potential low cost.

Mode-locked semiconductor lasers in monolithic and external-cavity architectures have been developed since 1980s and demonstrated stable femtosecond pulse generation with high repetition rates corresponding to the cavity length. So far, various types of mode-locked semiconductor lasers have been studied, such as monolithic passive-colliding-pulse-mode-locked quantum-well lasers^{1,2}, quantum-dots lasers³⁻⁷ and external-cavity active-mode-locked buried-heterostructure lasers^{8,9}. Recently, intra-cavity spectral shaping and dispersion control technologies enabled ultrashort pulses within a few hundred femtoseconds¹⁰⁻¹².

Gain-switched semiconductor lasers provide an alternative solution, which have performed shortest pulses of picoseconds duration since 1970s. Although the shortest pulses have been longer than that of the ML semiconductor lasers, the flexibility of the pulse shaping and also repetition rate and their high robustness are their unique strength¹³⁻¹⁵. In particular, gain-switched semiconductor lasers combined with rare-earth-doped fibre linear amplifiers in a master-oscillator-power-amplifier configuration have significant advantages because of the highly controllable optical pulses, such as variable repetition rate, arbitrary timing operation, flexible pulse duration, waveform spectral control and synchronization to electrical triggers, in addition to the robustness and stability¹⁶⁻²⁰. It was recently reported that additional non-linear pulse shaping in optical fibres can generate femtosecond pulses^{21,22}.

However, direct femtosecond pulse generation in gain-switched semiconductor lasers has never been achieved thus far for two reasons: (1) short-pulse generation via gain switching has been limited by the picosecond photon lifetime in laser cavities, and (2) the ultrafast non-linear carrier dynamics in semiconductors are complicated and difficult to control.

Here, we report novel gain-switched semiconductor-laser operation via an extreme optical pump, which can surpass the photon lifetime limit and generate unprecedented ultrashort pulses with a pulse width of 670 fs and peak power of 7.5 W. We analysed the intraband carrier inversion dynamics in semiconductor lasers under extreme excitation enabling short-pulse generation beyond the photon lifetime limit. The present experiment demonstrates the possibility of achieving practical femtosecond lasers based on gain-switched semiconductor technology.

Results

Overview of previous and present studies. Figure 1a numerically describes the conventional behaviour of gain switching on electrical stepwise and optical impulsive pumping, represented as blue and red curves, respectively. Regarding the stepwise electrical pumping that injects carriers continuously from $t = 0$, the optical gain increases gradually towards a saturation level²³. Meanwhile, the emission intensity increases and consumes massive carriers, which decreases the emission intensity. An oscillatory tail recognized as a relaxation oscillation to steady-state operation occurs because of the continuous pumping. In contrast, impulsive pumping, represented as red curves, generates the main pulse without a relaxation oscillation and, therefore, simplifies the pulse dynamics. The optical pumping is important to investigate the fundamental short-pulse limit in each device independently of the electrical frequency bandwidth limit on the current injection.

Figure 1b shows the shortest pulses of the gain-switched semiconductor lasers achieved in the past 40 years both via electrical and optical pumping²⁴⁻³⁹. Even with optical pumping, short-pulse generation has been restricted to picoseconds. Standard theories of gain-switched semiconductor lasers attribute this to the fall-time limit due to the photon lifetime, which is determined by the cavity length and reflectivity of the cavity mirrors³⁵⁻³⁹.

According to our most recent observation, a non-linear fast pulse component appears in the high-energy region of the pulsed

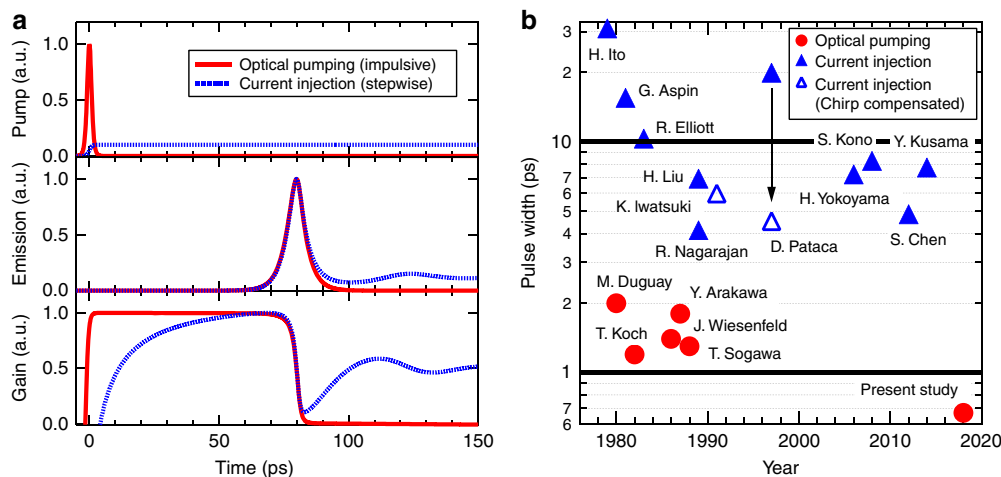


Fig. 1 Gain switching on electrical and optical pumping. **a** Conventional dynamics of gain switching operation with electrical stepwise and optical impulsive excitation numerically described as blue and red curves, respectively, in terms of the pump pulse, emission intensity and gain. **b** Record pulse widths of gain-switched semiconductor lasers reported in the last 40 years. The blue triangles and red circles indicate the electrical and optical pulsed excitation, respectively

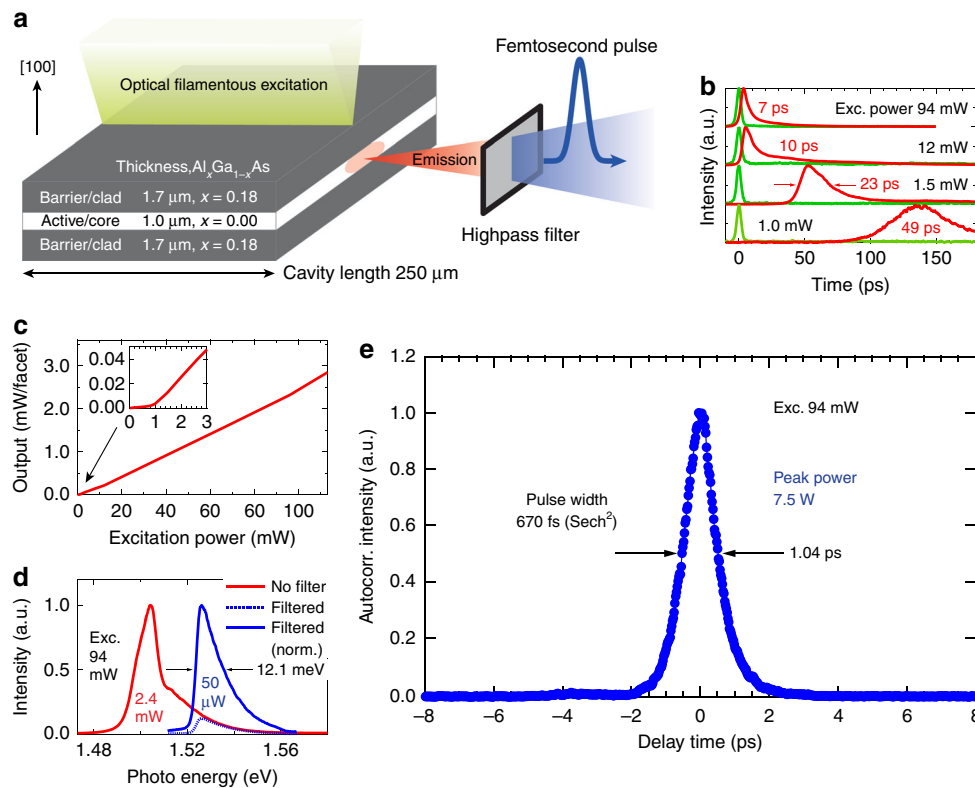


Fig. 2 Femtosecond pulse generation from the gain-switched semiconductor laser. **a** Schematic of the present gain-switched semiconductor laser consisting of an active GaAs layer (white) sandwiched between $\text{Al}_{0.18}\text{Ga}_{0.82}\text{As}$ layers (grey). A pulsed laser (green) of 1.59 eV is used for intense impulsive pumping. The pulsed emission (red) is due to the gain switching, where the high-energy component (blue) of the pulsed emission is extracted by a high-pass filter. **b** Time-resolved spectrally integrated emission (red curves) depending on the excitation power associated with the pump pulse waveforms (green curves). The emission is not spectrally resolved but includes its whole spectrum. **c** Excitation power dependence of the average output power of the full spectral waveguide emission. **d** Time-integrated energy spectra of the full waveguide emission and high-energy component after spectral filtering under an excitation power of 94 mW, plotted as red and blue curves, respectively. **e** Autocorrelation function of the high-energy component at an excitation power of 94 mW

spectrum on extreme intense excitation. Here, we study the gain switching dynamics initiated by the very strong pumping of 100 times the lasing threshold density and undoubtedly observe an unprecedented ultrashort-pulse width of 670 fs with a peak power of 7.5 W via autocorrelation measurement. The measured phenomena are reproduced effectively by our numerical calculation, which reveals the physical mechanism and true fundamental limit of the short-pulse generation.

Experimental setup. Figure 2a shows a schematic of the gain-switched semiconductor laser used in this study. It has a double-hetero (DH) structure consisting of a 1- μm -thick GaAs active layer sandwiched between $\text{Al}_{0.18}\text{Ga}_{0.82}\text{As}$ cladding layers grown by molecular beam epitaxy. We additionally tested several multiple-quantum-well structures, but the best result was obtained for the DH structure, which we report here. The cavity length was 250 μm , which gives a free spectral range and round-trip time of 0.6 meV and 6.9 ps, respectively. The photon lifetime τ_{ph} evaluated from the cavity length and reflectivity of 0.3 at the cleaved edge mirrors was 3.4 ps, and that including a cavity internal loss of 20 cm^{-1} was 2.3 ps.

We performed the impulsive excitation by optical excitation via our homemade ML fibre laser system, which provides a pulse width of 0.36 ps, photon energy of 1.59 eV, repetition rate of 10 MHz and average power of 0.33 W (see Methods, overview and basic elements of the fibre laser system for the configuration and characterization). The sample temperature was set at 5 K. Pumping light, with a 30% reflection loss at the top $\text{Al}_{0.18}\text{Ga}_{0.82}\text{As}$

surface, was incident on the sample in a filament shape with a spatial half-width of 1.7 μm along the cavity, by cylindrical and objective lenses. The uniformity of the excitation was within $\pm 15\%$ along the cavity. The average power of the pumping light before the reflection loss is referred to as the excitation power. The excitation light selectively pumped the GaAs layer because the band gap energies of the GaAs and $\text{Al}_{0.18}\text{Ga}_{0.82}\text{As}$ layers were 1.52 and 1.74 eV, respectively. The GaAs active layer absorbed 80% of the impulsive excitation light power instantaneously, giving rise to strong population inversion.

Femtosecond pulse generation. Figure 2b presents time-resolved measurements of the full spectral emission (red curves) with the pump pulses (green curve) scattered at the sample edge. It indicates that the laser emitted pulsed light because of the gain switching, where the zero on the time axis corresponds to the peak position on the green curves; the time resolution was 3 ps. The pulse width was tuned from 49 to 7 ps by increasing the excitation power from 1.0 to 94 mW.

Figure 2c plots the measured average output power of the gain-switched emission pulses per facet versus excitation power. The output power is almost proportional to the excitation power, which reaches 2.4 mW with an excitation power of 100 mW. The inset in Fig. 2c shows the near-threshold range from excitation powers of 0–3 mW, showing a lasing threshold of 0.9 mW.

We investigated the unique gain-switched lasing phenomenon for the extreme intense excitation power of 100 times the threshold. Figure 2d presents a time-integrated spectrum (red

curve) of the gain-switched pulses with an output of 2.4 mW and excitation power of 94 mW. The spectral resolution in the measurement was 3 meV. The spectrum is centred at 1.51 eV and anomalously broadened over 80 meV from 1.48 to 1.56 eV. The blue-dotted curve in Fig. 2d indicates the high-energy component above 1.52 eV extracted from the red curve by a high-pass filter inserted between the sample and detector. The centre of mass of the extracted spectrum is 1.53 eV and the integrated average power is 50 μ W. The blue solid curve in Fig. 2d represents the normalized spectrum for the blue-dotted curve with a full width at half-maximum (FWHM) of 12.1 meV. This spectral filtering is one of the key points in extracting ultrashort pulses beyond the photon lifetime limit. The reason or the mechanism enabling the ultrashort-pulse extraction by the spectral filtering will be shown later on the basis of pulse spectral dynamics.

Figure 2e shows the intensity-autocorrelation function measured after spectral filtering. The FWHM of the function is 1.04 ps, which ensures sub-picosecond pulse generation. The pulse width was estimated to be 670 fs from the sech^2 of the pulse shape on the time waveform. Consequently, the peak power was attained to be 7.5 W. Thus, we successfully demonstrated femtosecond pulse generation with a watt-class peak power by a gain-switched bulky Fabry–Perot semiconductor laser.

In the present measurements, the sample temperature was set at 5 K, because the sample cooling exaggerates characteristic features of the gain-switched pulses, which is helpful for clarifying the pulse dynamics and underlying physics breaking the photon lifetime limit. At 300 K, our gain-switched semiconductor laser generated 1.2 ps pulse width. Experimental data at 300 K, in comparison with those at 5 K, are summarized in Supplementary Table 1 (see also Supplementary Note 1 for the pulse dynamics at 300 K in details).

Pulse spectral dynamics. Table 1 summarizes the pulse widths, round-trip times and photon lifetimes of the present study compared with those of previous experiments. It can be seen that the pulses in previous reports are shorter than the round-trip times and close to the photon lifetimes, consistent with the short-pulse limitation of gain-switched semiconductor lasers or conventional theoretical models of single-mode rate equations. Interestingly, the pulse width of 670 fs in our present experiment is far shorter than the photon lifetime limitation of 3.4 ps. In this respect, the present femtosecond pulse generation is essentially different from conventional gain switching or those reported in other studies^{40,41}. Thus, we further investigated the full pulse spectral dynamics.

Figure 3 shows the excitation power dependence of the pulse spectral dynamics measured by a synchronous-scan-mode streak camera with a time and energy resolution of 3 ps and 3 meV, respectively (see Methods, time- and energy-resolved measurement system for the configuration and characterization).

Table 1 Summary of the pulse widths, round-trip times and photon lifetimes in comparison to previous measurements

	Pulse width (ps)	Round trip (ps)	Photon lifetime (ps)
Duguay et al. [35]	2.0	0.08	0.8
Koch et al. [36]	1.2	2.1	0.5
Arakawa et al. [38]	1.8	4.1	2.1
Present study	0.67	6.9	3.4

The pulse widths for previous reports are shorter than the round-trip times and close to the photon lifetimes with the short-pulse limit in the gain-switched semiconductor lasers. Remarkably, the pulse width measured in the present study is five times shorter than the photon lifetime and thus greatly exceeds the limitation

The spectra of Fig. 3a, b measured, respectively, at the weak excitation densities of 1 and 1.5 mW exhibit narrow bandwidths and featureless structures. The pulse widths and delay time decrease with excitation power. We note that conventional gain-switched lasing in single-mode rate-equation models can explain the spectral dynamics at low carrier densities, i.e., up to several times the lasing threshold density.

As shown in Fig. 3c at an excitation power of 12 mW (10 times higher than the lasing threshold), a fast component in the high-energy region of the spectrum appears and extends towards the high-energy region, particularly with the increase in excitation power. Finally, at an excitation power of 94 mW (100 times higher than the lasing threshold), we obtain a significantly broadened spectrum, as shown in Fig. 3d, where the fast component down-chirps from 1.56 to 1.48 eV, resulting in the bandwidth spread of 80 meV in Fig. 2d.

Figure 3e shows the spectral component filtered spectrally above 1.52 eV by a high-pass filter. Its energy-integrated waveform exhibits a FWHM of 3 ps on the streak camera, which is limited by its time resolution, and its proper pulse width was measured to be 670 fs by the autocorrelation experiment in Fig. 2e. The pulse width of the low-energy component at 1.50 eV is 17 ps, which is longer than the cavity photon lifetime of 3.4 ps.

Theoretical modelling. To interpret the observed phenomena, we performed theoretical calculations based on the rate equations,

$$\frac{df_{\alpha}(\varepsilon, t)}{dt} = f_{\alpha}^{\text{cf}} \delta(\varepsilon - \varepsilon_{\text{ex}}, t) - \frac{f_{\alpha}(\varepsilon, t) - f_{\alpha}^{\text{th}}(\varepsilon, T(t), \mu_{\alpha}(t))}{\tau_r} - \frac{v_g G(\varepsilon, t) \phi(\varepsilon, t)}{D(\varepsilon)}, \alpha = e, h \quad (1)$$

$$\frac{d\phi(\varepsilon, t)}{dt} = v_g G(\varepsilon, t) \phi(\varepsilon, t) - \frac{\phi(\varepsilon, t)}{\tau_{\text{ph}}} \quad (2)$$

for the non-equilibrium intraband carrier distribution $f_{\alpha}(\varepsilon, t)$ ($\alpha = e$ for electrons and h for holes) and multi-mode laser photon flux $\phi(\varepsilon, t)$ at energy ε and time t . The symbols in Eqs. (1) and (2) have usual meaning.

All the terms except for the second term in the right hand side of Eq. (1) are justified as necessary and/or usual terms: since the observed pulse dynamics depend both on energy ε and time t , we must at least introduce rate equations for the intraband carrier distribution $f_{\alpha}(\varepsilon, t)$, and laser photon flux $\phi(\varepsilon, t)$, as functions of both energy ε and time t . As in usual laser rate equations, we introduced the coupling terms via the gain coefficient $G \propto f_e + f_h - 1$, a cavity loss term with photon lifetime τ_{ph} , and a pumping term proportional to $\delta(\varepsilon - \varepsilon_{\text{ex}}, t)$.

The second term in the right hand side of Eq. (1) represents carrier thermalization term. Here, we assumed carrier thermalization via the carrier–carrier scattering mechanism, which thermalizes carriers among them with a finite carrier–carrier-scattering time constant τ_r ($=100$ fs)⁴². We also assumed that carrier cooling via phonon emission is irrelevant, and is omitted in Eq. (1).

This assumption was not the only choice. Indeed, in an early model³⁶ by Koch et al., they made opposite assumptions of infinitely fast carrier–carrier-scattering and finite carrier cooling due to optical-phonon emission mechanism. We first tested such assumptions, but we failed to reproduce our experimental results, showing a pulse width of 670 fs in a high-energy part shorter than the photon lifetime. Therefore, we now try our present model assuming the non-equilibrium carrier distribution with finite

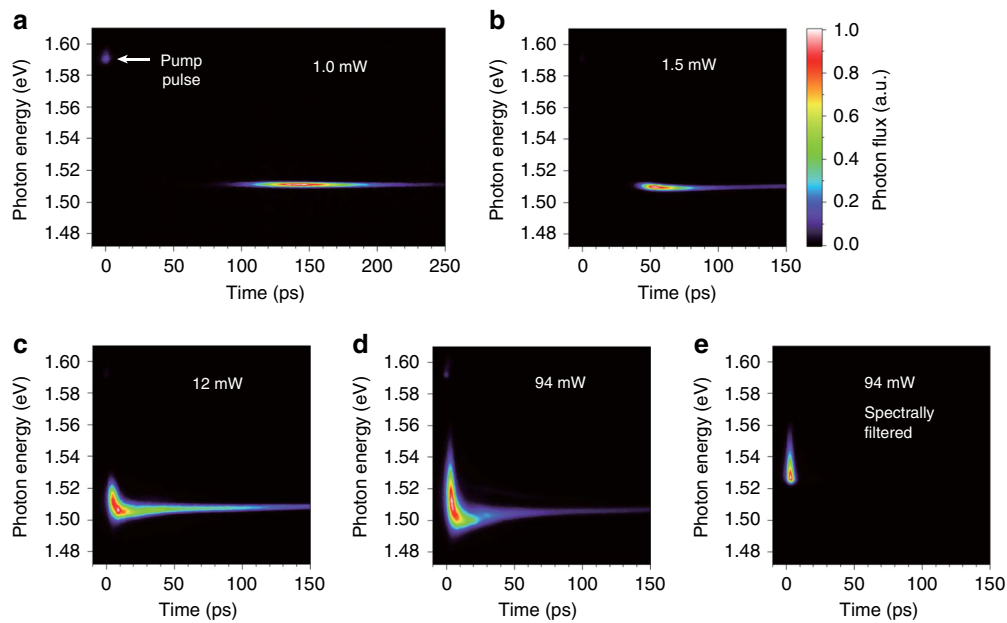


Fig. 3 Measurement of the pulse dynamics. **a–e** Observed spectral dynamics of the gain-switched pulses with various excitation powers by a synchronous-scan-mode streak camera with a time and energy resolution of 3 ps and 3 meV, respectively. The plots have been normalized to the photon flux, illustrated by the colour bar

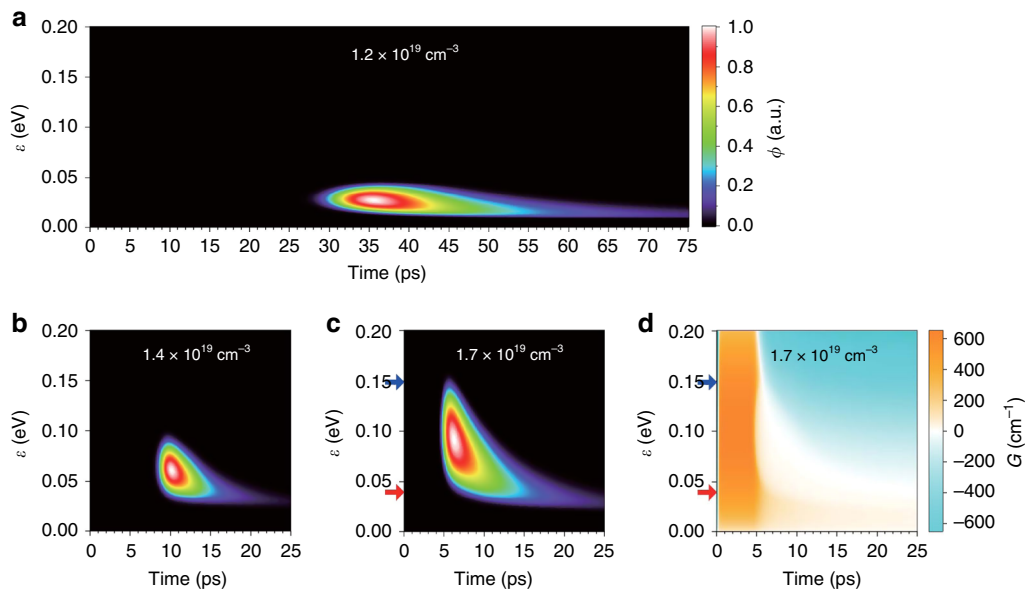


Fig. 4 Simulation of the pulse dynamics. **a–c** Calculated pulse spectral dynamics under different excitation carrier densities. The plots have been normalized to the photon flux, illustrated by the colour bar. **d** Calculated gain spectrum dynamics related to **c**. Note that the orange, white and cyan colours represent gain ($G > 0$), transparency ($G = 0$) and absorption ($G < 0$), respectively. In **c** and **d**, the blue and red arrows indicate the higher ($\epsilon = 0.149$ eV) and lower ($\epsilon = 0.040$ eV) energy regions of the spectrum

thermalization rate via carrier–carrier scattering time τ_r (see Supplementary Note 2 for the formulation, symbol definition and discussions on difference from previous theories).

Figure 4a–c present the calculated pulse dynamics $\phi(\epsilon, t)$ after impulsive excitation at $t = 0$ with different initial carrier densities, where ϵ measures the photon energy relative to the band gap energy. For the low-density excitation shown in Fig. 4a, the spectrum is featureless and exhibits a narrow width. The pulse width was long. As the excitation power increases, the pulse gradually decreases in width and delay, as shown in Fig. 4b. The spectrum starts spreading to the high-energy region. Eventually, a fast high-energy component appears, as shown in Fig. 4c.

Therein, the blue and red arrows indicate the high- and low-energy components of the pulse spectrum at $\epsilon = 0.149$ and 0.040 eV, respectively, for which the time profiles of ϕ are presented in Fig. 5a, b, respectively.

Note that the pulse width at the blue arrow is 1.1 ps, which is far shorter than the photon lifetime $\tau_{ph} = 3.4$ ps. The pulse width at the red arrow is 14 ps. The present simulation reproduces effectively the experimental features in the excitation density and photon energy dependence.

To understand the origin of the short-pulse generation beyond the photon lifetime limit in Fig. 4c, we depict the corresponding gain coefficient G in Fig. 4d. The time profiles of G at the blue and

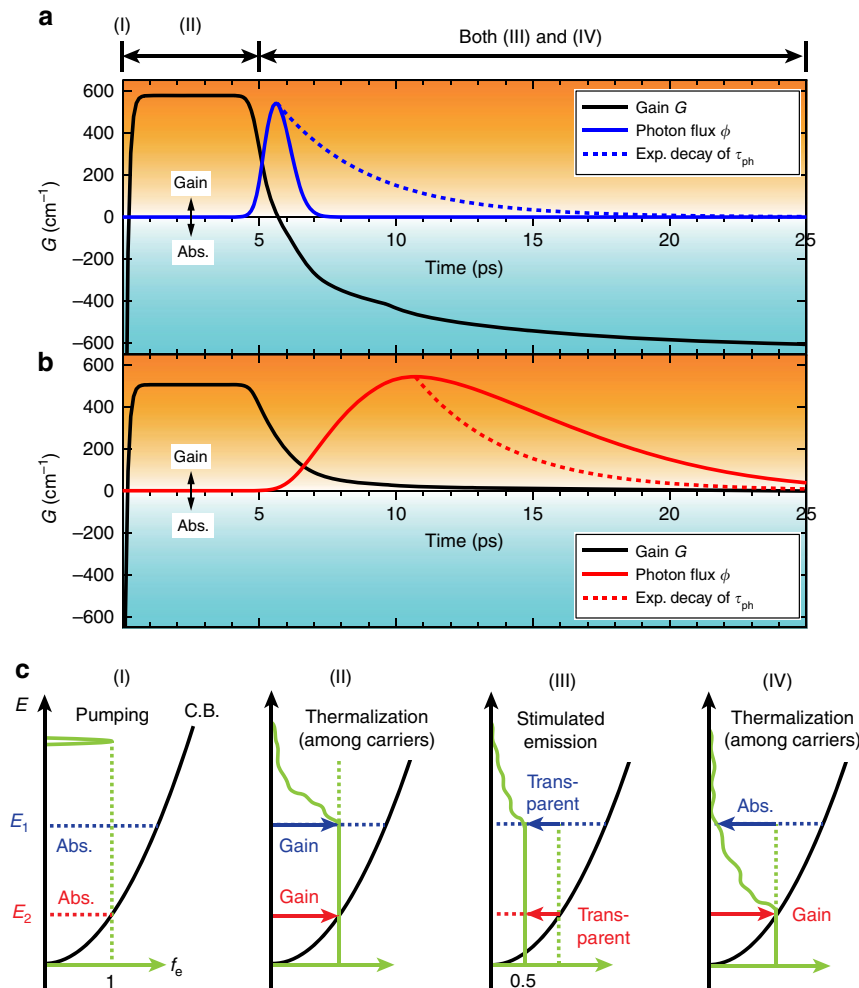


Fig. 5 Mechanism surpassing the photon lifetime limit. **a, b** Calculated time profiles of photon flux, ϕ , represented as blue and red solid curves in the higher ($\epsilon = 0.149$ eV) and lower ($\epsilon = 0.040$ eV) energy regions of the spectrum of Fig. 4c, respectively, where the dotted blue and red curves represent exponential functions of the decay constant $\tau_{\text{ph}} = 3.4$ ps. Herein, the black curves are time profiles of the gain coefficient G at the energy levels in Fig. 4d. **c** Schematic of the energy distribution functions of electrons f_e in the conduction band virtually separated into four regimes, (I), (II), (III), (IV), on the time axis for easy visualization. The green curves represent the distribution functions. The energy levels of E_1 and E_2 are associated with **a** and **b**, respectively

red arrow energies are presented in Fig. 5a, b, respectively. At the red arrow or low-energy $\epsilon = 0.040$ eV, G slowly changes from gain ($G > 0$, orange) to transparency ($G = 0$, white) in picoseconds. However, at the blue arrow or high-energy $\epsilon = 0.149$ eV, G changes rapidly from gain to absorption ($G < 0$, cyan) in less than a picosecond. When the laser cavity is transparent ($G = 0$), the decay time of laser emission should be equal to the photon lifetime τ_{ph} . As G at low-energy $\epsilon = 0.040$ eV is always positive ($G > 0$), the decay time is longer than τ_{ph} and the pulse width is limited by τ_{ph} . However, G at high-energy $\epsilon = 0.149$ eV rapidly becomes negative or absorptive ($G < 0$), which extinguishes photons in the cavity. Therefore, the decay time becomes shorter than τ_{ph} and the pulse width can surpass the photon lifetime limit.

Discussion

As for the mechanisms that make G change rapidly from gain to absorption only at high-energy $\epsilon = 0.149$ eV, our interpretation is illustrated in Fig. 5c, where we divide the carrier dynamics into four regimes from (I) to (IV). In regime (I), the high-density carriers are excited into the active layer by impulsive excitation at $t = 0$. In regime (II), ultrafast carrier–carrier scattering induces intraband thermalization among the carriers, by which

population inversion ($f_e \sim f_h \sim 1$) and, thus, a gain form over a wide energy region covering E_1 and E_2 . In regime (III), significant stimulated emission occurs rapidly and consumes carriers in the wide energy region covering E_1 and E_2 , which is just the typical gain switching operation. Note here that the gain switching reduces the carrier population only to a transparent density ($f_e \sim f_h \sim 0.5$). In regime (IV), ultrafast carrier–carrier scattering also induces intraband thermalization. As the total carrier density is lower than that in (II), absorption ($G < 0$) at high-energy E_1 and gain ($G > 0$) at low-energy E_2 are generated. In reality, (III) and (IV) occur simultaneously and repeatedly. However, these processes reasonably explain the mechanisms that make G change rapidly from gain to absorption at high energy and slowly from gain to transparency at low energy (see Supplementary Note 3 for more detailed explanations).

The above-explained mechanism under extremely intense excitation includes ultrafast non-linear carrier dynamics and is beyond conventional gain switching. Therein, the pulse width is limited by the amplitude of the gain coefficient and carrier–carrier scattering time, instead of the photon lifetime.

In conclusion, we first demonstrated femtosecond pulse generation with a pulse width of 670 fs and peak power of 7.5 W directly from a gain-switched semiconductor laser. It was

performed in a Fabry–Perot laser with a thick bulky active layer under extremely dense excitation. It differs from conventional gain switching in that the obtained pulse width of 670 fs is far shorter than the photon lifetime limit of 3.4 ps. Our theoretical analysis has demonstrated that carrier consumption by stimulated emission and ultrafast thermalization among the carriers by carrier–carrier scattering occur simultaneously and rapidly switch the gain to absorption in the high-energy region in the emission spectrum and enable short-pulse generation beyond the photon lifetime limit. The pulse width is limited by the carrier–carrier scattering time.

We believe the present study provides feasible designs for achieving practical femtosecond lasers at various photon energies. For instance, an electrically driven femtosecond gain-switched semiconductor laser operating at 1.24 eV (1.0 μm in wavelength) may be performed with our design strategy and combined with Yb-doped fibre linear amplifiers in the future. Such a novel master-oscillator-power-amplifier system based on the gain-switched semiconductor technology will inherit the highly controllable optical pulses with the robustness and stability (variable repetition rate, arbitrary timing operation, flexible pulse duration, waveform spectral control and synchronization to electrical triggers) and play a key role in prospective non-linear applications for industrial and social development.

Methods

Overview of the fibre laser system. Supplementary Figure 1a shows a schematic of our homemade chirped pulse amplification fibre laser system consisting of a 10-MHz-repetition-rate ML Er-doped fibre laser oscillator, pulse stretcher, Er-doped fibre amplifier as a pre-amp, ErYb-codoped fibre amplifier as a main amp, pulse compressor and second harmonic generator. Supplementary Figure 1b and c present the measured energy spectrum and intensity-autocorrelation function of the output from the laser system. The peak photon energy and spectral width of the FWHM are 1.589 and 4.28 meV, equivalent to 1.03 THz, respectively. The time width of the FWHM of the autocorrelation function is 550 fs, which corresponds to a pulse width of 360 fs. The maximum average output power is 0.33 W. Hence, the pulse energy per pulse, peak power and time-bandwidth product are 33 nJ, 90 kW and 0.37, respectively.

Supplementary Table 2 summarizes the output from the laser system with fundamental waves of 0.795 eV before photon energy conversion, which is explained in detail in Methods, basic elements of the fibre laser system, in comparison with a conventional ML Ti:Sapphire oscillator, which indicates that the output of the fibre laser system is three times as intense as that of the oscillator in terms of the energy per pulse.

Basic elements of the fibre laser system. As for the basic elements involved in Supplementary Figure 1a, the Er-doped fibre laser oscillator, which utilizes the passive mode-locking of non-linear polarization rotation, generates 830-fs pulses at a photon energy of 0.795 eV with a spectral width of 8.1 meV. The average output power is 2 mW. The pulse stretcher of a dispersion compensating fibre stretches the femtosecond pulse width to 88 ps to reduce the peak power and avoid non-linear effects in the following fibre amplifiers. The pre-amp based on an Er-doped single-mode fibre pumped by a laser diode at 1.27 eV, equivalent to 976 nm, amplifies the pulse intensity to an average of 29 mW. After the isolation blocking from backward pulses, the main amp, based on an ErYb-codoped single-mode-core double-cladding fibre and pumped at 1.27 eV, further increases the pre-amplified intensity and yields an average output power of 0.82 W. The pulse compressor consists of transparent-grating pairs in free space and compensates chromatic dispersion in the chirped pulses by compression to 450 fs with an average output power of 0.61 W and spectral width of 5.34 meV. The peak power is 140 kW. The second harmonic generator of a periodically poled lithium niobate crystal up-converts the fundamental waves of 0.795 eV to second harmonics of 1.589 eV. The average power and spectral width of the harmonics are 0.33 W and 4.28 meV, respectively. Thus, the conversion efficiency is 53%. Supplementary Table 2 summarizes these pulse characteristics.

Time- and energy-resolved measurement system. Supplementary Figure 2a shows a schematic of the time- and energy-resolved measurement system based on the fibre laser system of 10 MHz combined with a synchronous-scan-mode streak camera operating at 80 MHz, which enables the dynamical emission to be precisely characterized with time and energy resolutions of 3.4 ps and 3.0 meV, respectively. To synchronize the internal clock of 80 MHz installed in the streak camera with the laser system, we converted a small amount of output from the seeding ML oscillator to electric signals via a photodetector, which has a frequency comb structure

over a THz bandwidth in 10-MHz steps. A bandpass filter extracts the 80-MHz component from the comb and a radio-frequency amplifier increases the extracted signal voltage to an appropriate level for the external trigger. Supplementary Figure 2b presents the timing chart of the measurement, where the green and black curves represent the external triggers and synchronized sweeps in the streak camera, respectively. It should be noted here that the emission pulses originate from the sample at a repetition rate of 10 MHz, as shown by the orange curve.

Supplementary Figure 2c presents a time- and energy-resolved measurement for output pulses from the fibre laser system (pulse width of 360 fs and spectral width of 4.28 meV), where the sample in Supplementary Figure 2a is replaced with a mirror, which reflects pulses into the streak camera. Supplementary Figure 2d and e show an energy-integrated time waveform and time-integrated energy spectrum, respectively. In Supplementary Figure 2d, the FWHM of the time waveform including timing jitters of the external trigger is 3.4 ps, defined as the time resolution of the measurement system. The energy resolution has been determined to be 3.0 meV via the measurement of the bright line at 1.67 eV in the Ne lamp. As for Supplementary Figure 2e, the FWHM of the energy spectrum is 5.6 meV and is broader than the original spectral width of 4.28 meV because of the convolution with an energy resolution of 3.0 meV.

Data availability. The data that support the findings of this study are available from the corresponding authors upon request.

Received: 26 February 2018 Accepted: 4 July 2018

Published online: 08 August 2018

References

- Chen, Y., Wu, M., Tanbun-Ek, T., Logan, R. & Chin, M. Subpicosecond monolithic colliding-pulse mode-locked multiple quantum well lasers. *Appl. Phys. Lett.* **58**, 1253 (1991).
- Chen, Y. & Wu, M. Monolithic colliding-pulse mode-locked quantum-well lasers. *IEEE J. Quantum Electron.* **28**, 2176–2185 (1992).
- Rafailov, E. et al. Amplification of femtosecond pulses over by 18 dB in a quantum-dot semiconductor optical amplifier. *IEEE Photon. Technol. Lett.* **15**, 1023–1025 (2003).
- Rafailov, E. et al. Investigation of transition dynamics in a quantum-dot laser optically pumped by femtosecond pulses. *Appl. Phys. Lett.* **88**, 041101 (2006).
- Rafailov, E., Cataluna, M. & Sibbett, W. Mode-locked quantum-dot lasers. *Nat. Photon.* **1**, 395–401 (2007).
- Nikitichev, D. et al. High peak power and sub-picosecond Fourier-limited pulse generation from passively mode-locked monolithic two-section gain-guided tapered InGaAs quantum-dot lasers. *Laser Phys.* **22**, 715–724 (2012).
- Weber, C. et al. Picosecond pulse amplification up to a peak power of 42 W by a quantum-dot tapered optical amplifier and a mode-locked laser emitting at 1.26 μm . *Opt. Lett.* **40**, 395–398 (2015).
- Corzine, S. et al. Actively mode-locked GaInAsP laser with subpicosecond output. *Appl. Phys. Lett.* **52**, 348 (1988).
- Bowers, J., Morton, P., Mar, A. & Corzine, S. Actively mode-locked semiconductor lasers. *IEEE J. Quantum Electron.* **25**, 1426–1439 (1989).
- Quarterman, A. et al. A passively mode-locked external-cavity semiconductor laser emitting 60-fs pulses. *Nat. Photon.* **3**, 729–731 (2009).
- Döpke, B. et al. Self-optimizing femtosecond semiconductor laser. *Opt. Express* **23**, 9710–9716 (2015).
- Pilny, R. et al. Femtosecond semiconductor laser system with resonator-internal dispersion adaptation. *Opt. Lett.* **42**, 1524–1527 (2017).
- Birkin, D. et al. Near-transform-limited picosecond pulses from a gain-switched InGaAs diode laser with fiber Bragg gratings. *Appl. Phys. Lett.* **79**, 151 (2001).
- Riecke, S. et al. Picosecond spectral dynamics of gain-switched DFB lasers. *IEEE J. Quantum Electron.* **47**, 715–722 (2011).
- Wada, K., Kitagawa, N., Matsukura, S., Matsuyama, T. & Horinaka, H. Timing and amplitude jitter in a gain-switched multimode semiconductor laser. *Jpn. J. Appl. Phys.* **55**, 042702 (2016).
- Kanzelmeyer, S. et al. All-fiber based amplification of 40 ps pulses from a gain-switched laser diode. *Opt. Express* **19**, 1854–1859 (2011).
- Heidt, A. et al. 100 kW peak power picosecond thulium-doped fiber amplifier system seeded by a gain-switched diode laser at 2 μm . *Opt. Lett.* **38**, 1615–1617 (2013).
- Müller, A. et al. Diode laser based light sources for biomedical applications. *Laser Photon. Rev.* **7**, 605–627 (2013).
- Teppitaksak, A., Thomas, G. & Damzen, M. Investigation of a versatile pulsed laser source based on a diode seed and ultra-high gain bounce geometry amplifiers. *Opt. Express* **23**, 12328–12336 (2015).

20. Tokunaga, K., Fang, Y., Yokoyama, H. & Ozeki, Y. Generation of synchronized picosecond pulses by a 1.06- μm gain-switched laser diode for stimulated Raman scattering microscopy. *Opt. Express* **24**, 9617–9628 (2016).
21. Fang, Y., Chaki, T., Hung, J., Yamada, H. & Yokoyama, H. 1 MW peak-power subpicosecond optical pulse source based on a gain-switched laser diode. *Opt. Lett.* **41**, 4028–4031 (2016).
22. Fu, W., Wright, L. & Wise, F. High-power femtosecond pulses without a modelocked laser. *Optica* **4**, 831–834 (2017).
23. Ito, T. et al. Transient hot-carrier optical gain in a gain-switched semiconductor laser. *Appl. Phys. Lett.* **103**, 082117 (2013).
24. Ito, H., Yokoyama, H., Murata, S. & Inaba, H. Picosecond optical pulse generation from an r.f. modulated AlGaAs d.h. diode laser. *Electron. Lett.* **15**, 738–740 (1979).
25. Aspin, G., Carroll, J. & Plumb, R. The effect of cavity length on picosecond pulse generation with highly rf modulated AlGaAs double heterostructure lasers. *Appl. Phys. Lett.* **39**, 860 (1981).
26. Elliott, R., DeXiu, H., DeFreez, R., Hunt, J. & Rickman, P. Picosecond optical pulse generation by impulse train current modulation of a semiconductor laser. *Appl. Phys. Lett.* **42**, 1012 (1983).
27. Liu, H., Fukazawa, M., Kawai, Y. & Kamiya, T. Gain-switched picosecond pulse (<10 ps) generation from 1.3 μm InGaAsP laser diodes. *IEEE J. Quantum Electron.* **25**, 1417–1425 (1989).
28. Nagarajan, R., Kamiya, T., Kasukawa, A. & Okamoto, H. Observation of ultrashort (<4 ps) gain-switched optical pulses from long-wavelength multiple quantum well lasers. *Appl. Phys. Lett.* **55**, 1273 (1989).
29. Iwatsuki, K., Suzuki, K. & Nishi, S. Adiabatic soliton compression of gain-switched DFB-LD pulse by distributed fiber Raman amplification. *IEEE Photon. Technol. Lett.* **3**, 1074–1076 (1991).
30. Pataca, D. et al. Gain-switched DFB lasers. *J. Microw. Optoelectron.* **1**, 46–63 (1997).
31. Yokoyama, H. et al. Two-photon bioimaging with picosecond optical pulses from a semiconductor laser. *Opt. Express* **14**, 3467–3471 (2006).
32. Kono, S., Oki, T., Miyajima, T., Ikeda, M. & Yokoyama, H. 12 W peak-power 10 ps duration optical pulse generation by gain switching of a single-transverse-mode GaInN blue laser diode. *Appl. Phys. Lett.* **93**, 131113 (2008).
33. Chen, S. et al. Sub-5-ps optical pulse generation from a 1.55- μm distributed-feedback laser diode with nanosecond electric pulse excitation and spectral filtering. *Opt. Express* **20**, 24843–24849 (2012).
34. Kusama, Y. et al. 7-ps optical pulse generation from a 1064-nm gain-switched laser diode and its application for two-photon microscopy. *Opt. Express* **22**, 5746–5753 (2014).
35. Duguay, M., Damen, T., Stone, J., Wiesenfeld, J. & Burrus, C. Picosecond pulses from an optically pumped ribbon-whisker laser. *Appl. Phys. Lett.* **37**, 369 (1980).
36. Koch, T., Chu, L., Harder, Ch & Yariv, A. Picosecond carrier dynamics and laser action in optically pumped buried heterostructure lasers. *Appl. Phys. Lett.* **41**, 6 (1982).
37. Wiesenfeld, J. & Stone, J. Picosecond pulse generation in optically pumped, ultrashort-cavity, InGaAsP, InP, and InGaAs film lasers. *IEEE J. Quantum Electron.* **22**, 119–132 (1986).
38. Arakawa, Y., Sogawa, T., Nishioka, M., Tanaka, M. & Sakaki, H. Picosecond pulse generation (<1.8 ps) in a quantum well laser by a gain switching method. *Appl. Phys. Lett.* **51**, 1295 (1987).
39. Sogawa, T., Arakawa, Y., Tanaka, M. & Sakaki, H. Observation of a short optical pulse (<1.3 ps) from a gain-switched quantum well laser. *Appl. Phys. Lett.* **53**, 1580 (1988).
40. Vasil'ev, P. *Ultrafast Diode Lasers: Fundamentals and Applications* (Artech House, Norwood, 1995).
41. Cong, K. et al. Dicke superradiance in solids. *J. Opt. Soc. Am. B* **33**, C80–C101 (2016).
42. Shah, J. *Hot Carriers in Semiconductor Nanostructures: Physics and Applications, 1st Edition* Ch. IV (Academic Press, San Diego, 1992).

Acknowledgements

This work was partly supported by KAKENHI no.15H03968 from JSPS, APSA and NEDO in Japan.

Author contributions

T.I. designed the project, designed the laser sample structure, developed the fibre laser system, performed the measurements, analysed the experimental results and wrote the paper. H.A. organized the contribution to the project and supervised the experiments, the analysis and writing of the paper. H.N., Y.H., T.N., S.C. and M.Y. equally contributed to the analysis of the theoretical modelling and physical interpretation in diverse points of view. H.N. further supported the measurements. C.K. fabricated the sample. Y.K. contributed significantly to the development of the fibre laser system.

Additional information

Supplementary information accompanies this paper at <https://doi.org/10.1038/s42005-018-0045-0>

Competing interests: The authors declare no competing interests.

Reprints and permission information is available online at <http://npg.nature.com/reprintsandpermissions/>.

Publisher's note: Springer Nature remains neutral with regard to jurisdictional claims in published maps and institutional affiliations.



Open Access This article is licensed under a Creative Commons Attribution 4.0 International License, which permits use, sharing, adaptation, distribution and reproduction in any medium or format, as long as you give appropriate credit to the original author(s) and the source, provide a link to the Creative Commons license, and indicate if changes were made. The images or other third party material in this article are included in the article's Creative Commons license, unless indicated otherwise in a credit line to the material. If material is not included in the article's Creative Commons license and your intended use is not permitted by statutory regulation or exceeds the permitted use, you will need to obtain permission directly from the copyright holder. To view a copy of this license, visit <http://creativecommons.org/licenses/by/4.0/>.

© The Author(s) 2018